Electrostatic actuation of nanomechanical optical fibers with integrated electrodes

Nina Podoliak*, Zhenggang Lian, Martha Segura, Wei H. Loh, and Peter Horak
Optoelectronics Research Centre, University of Southampton, Southampton, SO17 1BJ, U.K.

ABSTRACT

We investigate theoretically and experimentally the possibility of electrostatic actuation of nanomechanical optical fibers with integrated electrodes. The fiber has two optically guiding cores suspended in air by thin flexible membranes. This fiber structure allows for control of the optical properties via nanometer-range mechanical core movements. The electrostatic actuation of the fiber is generated by electrically charged electrodes embedded in the fiber cladding. Fiber designs with one to four electrodes are analyzed and, in particular, a quadrupole geometry is shown to allow for all-fiber optical switching in a 10cm fiber with an operating voltage of 25 - 30V. A multi-material fiber draw technique is demonstrated to fabricate a fiber with well-defined dual core structure in the middle and four continuous metal electrodes in the cladding. The fabricated fiber is analyzed and compared with the modeled requirements for electrostatic actuation.
Keywords: Microstructure optical fibers; MEMS devices; Optical switching.

1. INTRODUCTION

Developing devices for effective signal manipulation in the optical format currently attracts a lot of interest as this could offer huge advantages in the improvement of information processing and development of all-optical telecommunication networks. A particularly attractive option is provided by optical micro- and nano-electromechanical systems (MEMS and NEMS)[1]. Many optical MEMS devices contain moving membranes or mirrors with light propagating in free space[2], while others are based on light confined in moving optical waveguides[3]. Here we investigate the possibility of equivalent electrically controlled mechanical systems based on glass optical fibers, which can combine signal transmission and control functionalities. Such fiber devices would allow for easy integration with other fiber components and thus could become an essential part of reconfigurable all-fiber optical networks.

MEMS usually contain two main functional components: the mechanical part that can move, rotate or vibrate; and the actuation mechanism that controls the mechanical part. Nowadays MEMS are mainly fabricated on silicon chips, however the potential of glass-based MEMS has also been investigated[4], and several groups have already demonstrated electrostatic glass actuators[5,6]. In recent years, different research groups have fabricated multi-material fiber-based devices with integrated conducting wires by pressurizing low melting temperature metal alloy into the holes of microstructured optical fibers[7-9] or by deposition of semiconductors and metals into them from chemical precursors[10]. However, this type of post-processing is usually a time consuming approach and limits the device size. A multi-material co-draw technique was demonstrated by fabricating structural metal-insulator-semiconductor fibers with metal wires of a diameter below 10 μm[11]. Also a fiber with a single internal electrode and an electrically conductive coating was fabricated by feeding metal wires during fiber drawing[12].

In previous work[13,14] we have demonstrated a nanomechanical optical fiber with a suspended dual-core structure that allows for control of the optical properties via nanometer-range mechanical movements. The mechanical reconfiguration was achieved by controlling the gas pressure inside an air hole of the fiber. However, for various applications in telecommunications, sensing, or imaging, a faster and more robust actuation method is desirable. We therefore focus here on an electrostatic actuation mechanism in the dual-core fiber. This optical system is the fiber equivalent of chip-based optical MEMS switches incorporating two evanescently coupled waveguides as demonstrated recently in silicon[15] and InP[16]. Comb actuators are the most common actuation method for sub-micron sized guiding beams and waveguides on chips[17]. However, other methods have been recently introduced, including electrostatic actuation by means of a voltage applied directly to the waveguides[16] or by placing them in a non-uniform electric field created by nearby electrodes[18]. We demonstrate that the latter method can be realized inside optical fibers by integrating charged metal wires into the cladding. This can give a direct way to control light propagation in the dual-core fiber, leading to MEMS-type functionality in the system.

2. FIBER DESIGN

2.1 Optical properties of the fiber

Our nanomechanical optical fiber consists of two elliptical guiding cores independently suspended by thin and flexible glass membranes in a central air hole as schematically shown in Figure 1a. This fiber structure allows the cores to move with respect to each other. The cores are separated by a small air gap, remaining optically coupled through their overlapping evanescent fields. The fiber modal structure depending on the core size and the air gap between cores was analyzed by a full vectorial Finite Element Method (FEM) using Comsol Multiphysics® (RF module). We assumed a fiber made of lead silicate glass (Schott F2, refractive index n=1.6) and a wavelength of 1550 nm.

A fiber core size of 0.8×2 µm was assumed in the calculations taking the dimensions of a previously fabricated fiber[14], an SEM picture of which is shown in Figure 1a. Analysis of the modal structure shows that the individual fiber core supports four modes. The lowest order TE- and TM-like modes with predominant horizontal and vertical polarization, respectively, are shown in Figure 1b. When two cores are placed close to each other, the individual core modes become coupled, forming symmetric and antisymmetric superposition modes (or 'supermodes', see inset in Figure 1c), and their effective indices split. The supermode indices are highly sensitive to the air gap between the cores, *g*, with the mode index difference between the symmetric and antisymmetric supermodes decaying approximately exponentially with *g*, as shown in Figure 1c. Thus, by changing the separation between the cores it is possible to control the effective mode indices and in this way to tune the fiber optical properties.

We also analyzed the range of mode index variation depending on the core dimensions. The core width was varied in the range from 0.5 to 1 µm, keeping the core aspect ratio (core length to width) fixed at 2.5. The air gap in these calculations was varied between 0 and 2.5 µm. The variation of the mode index difference between the symmetric and antisymmetric TE_{00} modes induced by one nanometer gap change is shown in Fig 1d. For the TM_{00} mode a qualitatively similar behavior is found in the studied parameter region. By decreasing the individual core size the coupling strength and hence mode index difference increases, as the mode field spreads outside the cores. This figure clearly maps a range of fiber parameters where the index difference between symmetric and antisymmetric modes varies substantially with the gap size (of the order of 10^{-3}-10^{-4} for a nanometer gap variation) which allows for significant NEMS-type functionality.

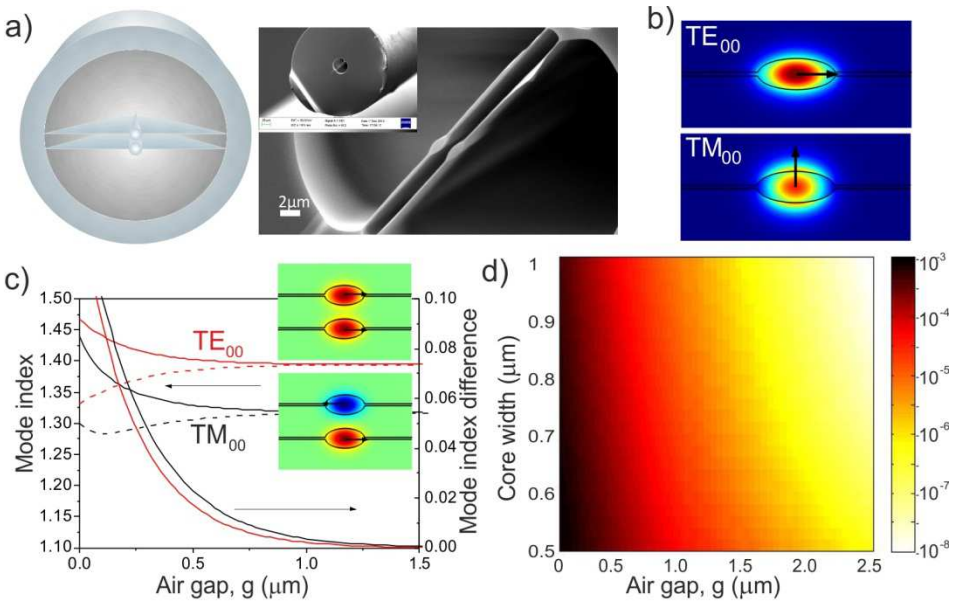

Figure 1. (a) Schematic of a fiber cross section and SEM image of a fabricated fiber. (b) Electric field distribution and predominant polarization of TE- and TM-like fundamental modes in a single core. (c) Effective mode indices of the TE_{00} and TM_{00} supermodes (solid and dashed lines correspond to symmetric and antisymmetric modes) and mode index difference between symmetric and antisymmetric modes of the dual core fiber with core size of 0.8×2 µm depending on the air gap between the cores. Inserts: Symmetric and antisymmetric TE_{00} supermodes. (d) Variation of mode index difference between symmetric and antisymmetric TE_{00} mode induced by 1 nm gap variation for a range of core sizes and air gaps.

2.2 Mechanical properties of the fiber

Neglecting the guiding cores, the supporting membranes can be modeled as doubly clamped beams, and using the classical Euler-Bernoulli beam equation[17] we get the core displacement induced by a unit force per unit fiber length, $\Delta g/F$, as:

$$\frac{\Delta g}{F} = \frac{1}{2E}\left(\frac{L_m}{h}\right)^3, \tag{1}$$

where L_m is the membrane half-length and h is its thickness, E is Young's modulus of the material. The induced core displacement is entirely determined by the supporting membrane material and dimensions and can thus be tailored by optimizing the fiber mechanical properties. Using Equation (1) for a membrane with $2L_m$ = 25 µm, and h = 0.1 µm, made of F2 glass (E = 57 GPa) we find that a force of 10^{-3} N/m can move a core by 17 nm. By making the membrane half as thick or twice as long, it is possible to increase the fiber mechanical response by almost an order of magnitude. The mechanical vibration frequency scales with the membrane size as $f \sim h/L_m^2$. However, it also depends on the core dimensions, since a large core with higher mass decreases the vibration frequency. For the previously reported fabricated range of fiber dimensions, the vibration frequencies were in the range of 0.5 – 10 MHz[13,14].

2.3 Electrostatic actuation and electrode design

To induce electrostatic actuation of the nanomechanical optical fibers we consider metallic wire electrodes in the fiber cladding. Two mechanisms were found to contribute significantly[19]. The charged electrodes induce electrical dipoles in the fiber cores and subsequently create gradient forces on them due to the non-uniform background field, which are also known as dielectrophoretic forces[20]. The induced dipoles of the two cores also interact directly through the dipole-dipole interaction that becomes dominant over short distances. In the following these two forces are described separately.

We first present a simplified analytical model to qualitatively characterize the electrostatic forces generated by a non-uniform electric field $\boldsymbol{E}_0$ on dielectric waveguide cores of circular cross-section. In particular, we concentrate on the relative force between the two cores depending on the distance d between their centers. The dielectrophoretic force, $\boldsymbol{F}_{el}$, depends on the external field gradient as

$$\boldsymbol{F}_{el} = (\boldsymbol{p}\cdot\boldsymbol{\nabla})\boldsymbol{E}_0 = a\,\varepsilon_0\,\frac{\varepsilon-1}{\varepsilon+1}\boldsymbol{\nabla}E_0^{\,2}, \tag{2}$$

were a is the core cross section and ε is the material dielectric constant. Thus, the relative force to lowest order in d dependents on the second derivative of the field squared and is linearly proportional to d:

$$\Delta F_{el} = F_{el1} - F_{el2} = a\,\varepsilon_0 d\,\frac{\varepsilon-1}{\varepsilon+1}\frac{\partial^2}{\partial y^2}E_0^{\,2}. \tag{3}$$

The dipole-dipole attractive force between the cores with induced dipole moments $\boldsymbol{p}_1$ and $\boldsymbol{p}_2$ (projection on axis y connecting the two cores) is proportional to d^{-3}:

$$F_d = (\boldsymbol{p}_2\cdot\boldsymbol{\nabla})E_1 = -\frac{1}{\pi\varepsilon_0}\frac{p_1 p_2}{d^3} \cong \frac{4a^2}{\pi}\varepsilon_0\frac{(\varepsilon-1)^2}{(\varepsilon+1)^2}\frac{E_0^{\,2}}{d^3}. \tag{4}$$

Noting that the background field strength E_0 is linearly proportional to the voltage applied to the electrode, both forces and, hence, the induced core displacements are proportional to the square of the voltage.

In the simplest geometry, we consider a single electrode of 15 µm diameter introduced into the fiber cladding with a 4 µm separation between the electrode edge and the central air hole edge (see Figure 2c). The electric field strength generated inside the central air hole was calculated numerically using the electrostatic module of Comsol Multiphysics®. The material dielectric permittivity ε~10 (typical for lead silicate glasses) was assumed. The electric field strength was then substituted into Equations (2) – (4). The corresponding dielectrophoretic forces acting on the top and bottom cores, the dipole interaction force, and the total forces acting on each of the cores depending on the separation between them at a fixed voltage are shown in Figure 2a. For small distances between the core centers, the attractive dipole-dipole interaction dominates. The absolute value of the total force decreases rapidly with increasing distance as predicted by

Equation (4). At larger distances the interaction with the external field dominates, and both cores are pulled into the same direction, towards the wire, but with slightly different forces. The force acting on the top core is larger than the force acting on the bottom core due to the difference in the external field gradient. So, for large gaps the relative force pulls the cores apart with a magnitude that increases linearly with increasing separation between the cores as predicted by Equation (3). Note that for this electrode geometry an intermediate distance exists where both cores experience the same force, so the relative separation between the cores does not change regardless of the magnitude of the applied voltage.

Next, we investigate how electrostatic forces depend on core dimensions. Figure 2b demonstrates electrostatic forces calculated for a fiber with smaller core sizes, namely 0.6×1.2 µm. The relative forces are compared in Figure 2d. In general, the absolute value of the forces is lower for the smaller cores. The analytical model suggests that the dielectrophoretic force depends linearly on core cross-section, a, while the dipole-dipole interaction force is proportional to a^2, (see Equations (2) and (4)). A larger difference is thus observed at smaller distances where the displacement is caused by the dipole-dipole attraction. Moreover, the point where the effects of the dielectrophoretic forces and the dipole-dipole forces cancel and the relative force is zero occurs at a smaller distance.

Equations (2) – (4) can be used to analyze the effect of the material dielectric constant on the induced forces. Figure 2d compares the absolute value of the relative forces for fibers of the same core size and made of different glasses (lead silicate glass and silica glass). The dielectric constant is included in Equations (2) – (4) in the ratio $(\varepsilon-1)/(\varepsilon+1)$, which at $\varepsilon >> 1$ becomes independent of ε and converges to 1. For smaller ε the ratio is less than 1, and the electrostatic forces thus decrease. Moreover, having a material with a lower dielectric constant around the central air hole decreases the field strength inside the hole. The electric field squared in the middle of the air hole calculated for the lead silicate and silica glasses are 1.60 and 1.31 V^2 μm^{-2}, and the corresponding first and second derivatives of $|E_0|^2$ are 0.14 and 0.11 V^2 μm^{-3}, and 0.017 and 0.016 V^2 μm^{-4}, respectively. Overall, Figure 2d thus shows a decrease in the relative force for a lower-index glass.

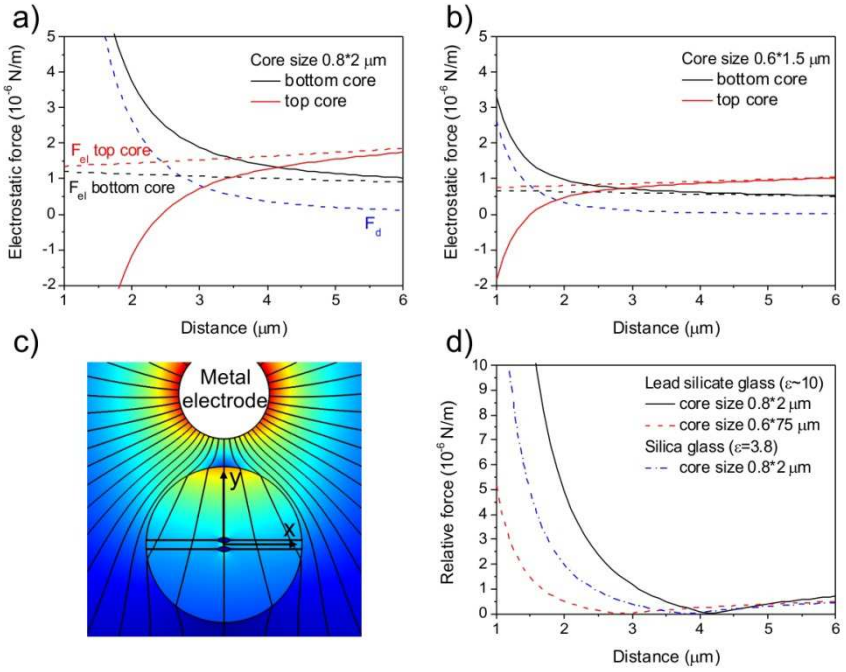

Figure 2. Electrostatic forces per unit fiber length acting on the top and bottom core depending on the initial distance between core centers calculated for fibers made of lead silicate glass with one electrode and core size of 0.8×2 µm (a) and 0.6×1.5 µm (b). (c) Fiber electrode geometry and electric field profile. (d) Relative force between two cores calculated for different core sizes and fiber glasses. A voltage of V = 50 Volts is assumed in all calculations.

The analytically calculated forces acting on the cores could be used to calculate the induced displacements of the cores using Equation (1). However, as was shown in our recent work[19], membranes perform not only the passive role of supporting the cores but, being made of the same material as the cores, they can also be polarized and experience forces.

Moreover, even if the membranes are much thinner than the cores, owing to their long lengths the membrane lateral cross-sections can be comparable to or even larger than the core areas with a correspondingly significant contribution to the forces. This makes the mechanical deformation mode of membranes more complex than bending of a doubly clamped beam. To account for these effects, we calculated core displacements using fully numerical FEM simulations in the MEMS Module of COMSOL Multiphysics®. Here we again assumed elliptical cores of size 0.8×2 µm and supporting membranes of thickness 0.1 µm and length 25 µm. This module calculates both the electrostatic forces distributed along the membranes and cores and the induced deformation of movable parts of the system. The model suggests that the core displacements induced by a single electrode is small, making the relative core displacements even smaller (see Figure 3b). The electrostatic forces, and hence the core displacements, can be maximized by increasing the electric field gradient. We thus investigated alternative fiber geometries with three and four electrodes in the vicinity of the fiber core (see Figure 3a). The square of the electric field strength, and the first and second derivative of $|E_0|^2$ in the center of the air hole (at $x = 0$ and $y = 0$) are given in Table 1. The comparison between relative displacements of the cores for all electrode geometries depending on the initial distance between the core centers is shown in Figure 3b.

Table 1. Electric field squared and the first and second derivative of the electric field squared in the center of the air hole calculated for electrode geometries shown in Figures 2c and 3a.

Fiber geometry	$\lvert E_0\rvert^2$, V^2 µm^{-2}	$\partial(E_0^2)/\partial y$, V^2 µm^{-3}	$\partial^2(E_0^2)/\partial y^2$, V^2 µm^{-4}
1 electrode	1.60	0.14	0.017
3 electrodes	11.12	1.03	0.045
4 electrodes	0	0	0.412

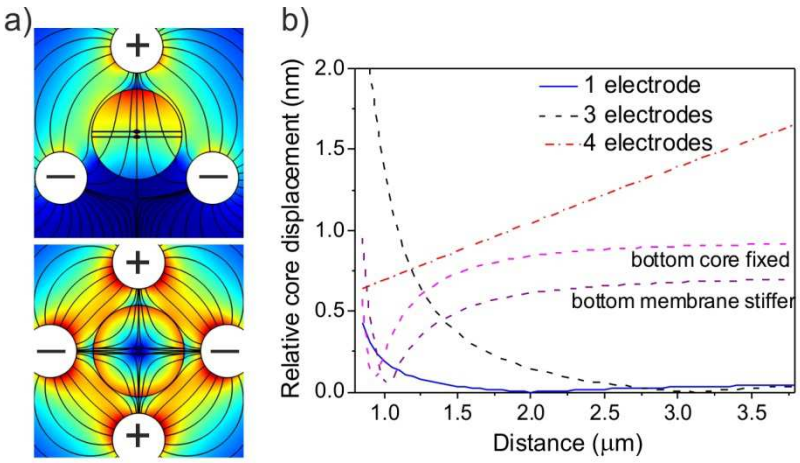

Figure 3. (a) Three-, and four- electrode configurations and electric field profile created inside the fiber. (b) Relative core displacement depending on the distance between their centers calculated numerically for fibers with the core size of 0.8×2 µm and supporting membranes of 0.1 µm thickness and 25 µm length. In all calculations V = 50 Volts.

Despite a significantly larger field and field gradient generated by three electrodes in comparison to one electrode, an improvement in the absolute value of the relative core displacement is observed only for small distances. The second derivative of $|E_0|^2$ is hardly larger, suggesting only a small increase of the relative movement between the cores, Equation (3). This means that the dielectrophoretic forces acting on the individual cores in the three-electrode geometry are much higher than those in the one-electrode configuration, but they move both cores in the same direction and hence give a small relative core displacement in a fiber with identical membranes. However, if one of the supporting membranes is stiffer than the other, similar forces introduce different displacements of the cores (see Equation (1)). This is demonstrated by numerical simulations of a fiber where the bottom membrane is twice as thick as the top one. An improvement of the relative core displacement by more than an order of magnitude is demonstrated by this method (see Figure 3b). Further increase of the membrane thickness can lead to the case where the bottom core does not move at all.

The relative core displacement then is determined by the force acting on the other core, and a further increase in the relative core displacement is shown in the figure in this case.

The four-electrode configuration yields qualitatively and quantitatively different behavior of the relative core displacement. This geometry generates an electric quadrupole field with zero field strength at the center of the fiber. Thus for small core separations, no dipole moments are induced and thus the dipole-dipole interaction vanishes. The displacements of the cores are therefore always dominated by the dielectrophoretic forces. The field gradient changes sign in the middle of the air hole, and the dielectrophoretic forces act in opposite directions if the cores are placed at the center of the fiber. The quadrupole field also exhibits the largest second derivative of $|\boldsymbol{E}_0|^2$ (see Table 1) leading to the largest relative forces and hence the largest core displacements of all geometries at the same voltage V for distances above 1.5 µm. Relative core displacements greater than one nanometer are predicted in this case, which would be sufficient to introduce changes to the optical properties.

3. OPTICAL SWITCHING IN A DUAL-CORE FIBER

As an example of fiber NEMS functionality, we demonstrate an optical switch based on the dual core fiber. The two fiber cores form a directional coupler. If an optical signal is launched into one of the cores, it will continuously switch between the cores while propagating along the fiber. The beat length, L_b, (propagation distance at which the light transfers from one core to the other and back) depends on the mode index difference between the symmetric and antisymmetric supermodes, n_s and n_a, and the wavelength λ as $L_b = \lambda / (n_s - n_a)$. As was shown above, moving the cores even by a sub-nanometer distance has a noticeable effect on supermode indices. Thus, varying the gap size changes the beat length of the coupled core modes and the output at the fiber end can be switched continuously between the two cores. The required change of the air gap Δg_s to switch light to the other core and back in a fiber of length L is given by

$$\Delta g_s = \frac{\lambda}{L \frac{\partial (n_s - n_a)}{\partial g}}, \qquad (5)$$

where the variation of the mode index difference with gap $\partial (n_s - n_a) / \partial g$ was given in Figure 1d. We also note from Equation (5) that $\Delta g_s \propto 1/L$, meaning increased fiber sensitivity to core movement with an increase of its length. Figure 4 shows the output of one core calculated for a 10 cm long fiber with the four-wire geometry, core size of 0.8×2 µm, and initial edge-to-edge separation of 0.7 µm. In this configuration, a complete switch of the light from one core to the other can be achieved at ~±25 Volts for the TM_{00} mode and ~±30 Volts for the TE_{00} mode inducing a relative core displacement of approximately 0.3 nm. For a shorter, 2.7 cm piece of fiber the optical switch requires higher voltage of ~±50 Volts, which will introduce a core displacement of 0.9 nm.

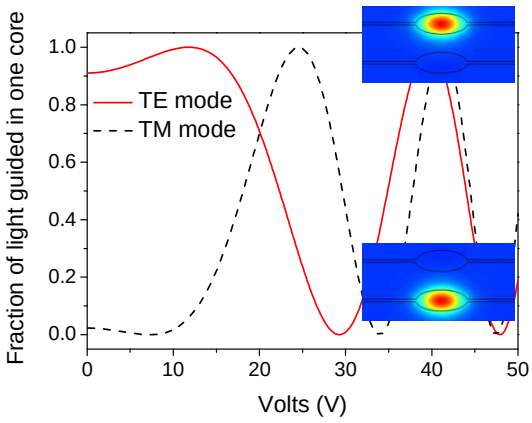

Figure 4. Variation of output intensity from one of the cores depending on applied voltage for a fiber with four wire geometry and with 0.7 µm initial air gap between the cores. A fiber length of L = 10 cm was assumed in the calculation.

4. FIBER FABRICATION AND CHARACTERIZATION

Based on the analysis above, we focused on the fabrication of a dual core fiber with quadrupole electrode configuration. Lead-silicate glass (Schott F2) was selected as a fiber core material and low melting temperature tin for the electrode wires. A dual core preform for the fiber central part was fabricated by the extrusion technique using a custom-designed stainless steel die. The preform was then drawn into a fiber cane[13,14]. To assemble the quadrupole electrode configuration, the cane was surrounded by four glass tubes filled with tin wires in the middle of a F2 jacket tube (10/8mm OD/ID). Four extra glass rods were added to secure the position of the cane and electrode wires, as shown in Figure 5a.

The multi-material stacked preform was drawn into a fiber in two steps on a fiber drawing tower. In the first step, the preform was pre-heated to a temperature above the melting temperature of tin (230ºC) for 60 minutes. The melted tin condensed down to the bottom of the preform, removing air bubbles between the metal and the glass, thus avoiding discontinuous wires in the fiber. In the second step, the fiber was fabricated using a drawing temperature of 730ºC.

An SEM image of the first fiber sample is shown in Figure 5b. The fiber OD is 200 µm and the average diameter of the four tin wires is 50 µm. Tens of meters of fiber were fabricated with relatively uniform cores and continuous electrodes along the fiber. The total resistance of the four electrodes was measured to be 19.6 Ω/m. The dual core structure is well centered between the four electrodes. Figure 5c shows a magnification of the two suspended cores in the center of the fiber. From this, we obtain the dimensions of the fabricated structure: The core size is 2.0×3.1 µm, the membranes are 12 µm long and 500 nm thick, and the air gap between the cores is ~200 nm. The optical loss of the fiber measured by the cut-back method for TE and TM polarizations was found to be 2.5 and 4.8 dB/m respectively.

Figure 5. (a) Stacked preform of the dual core fiber with quadrupole metal electrodes; (b) SEM picture of the fabricated fiber, scale bar is 10 µm. (c) Magnification of the fiber central part demonstrating two suspended cores, scale bar is 2 µm.

We modified the geometries in the optical and electromechanical numerical models to resemble the actual fabricated fiber from Figure 5. The analysis of the fiber optical modes shows that even though the core dimensions are relatively large, their close position ensures good optical coupling between the cores. A variation of the index difference between symmetric and antisymmetric TE polarized supermodes of 2.5×10^{-5} is expected with a nanometer change of the air gap. However, the supporting membranes in these first fabricated fibers turned out to be too stiff to allow for sufficient core movements at realistic voltages. The electromechanical model suggests that a voltage higher than ±200 Volts has to be applied to the electrodes to observe switching in a 50 cm long piece of the fiber. This voltage, however, generates an electric field inside the fiber well above the dielectric strength of air and will thus lead to dielectric breakdown. Using the numerical model we found that by reducing the membrane thickness to 200 nm and increasing its length to 25 µm the switching voltage could be reduced to more realistic ±35 Volts.

Our next attempts will thus focus on adjusting the fabrication process in order to reduce the mechanical stiffness by making the membranes longer and thinner. The SEM image in Figure 5b suggests that the size of the central part with the suspended cores is not yet restricted by the electrodes. Membranes of the required dimensions have also been fabricated previously, thus we expect that pressurizing the fiber cane during the drawing process will help us to achieve the target fiber dimensions.

5. CONCLUSIONS

In conclusion, we have investigated the concept of electrostatic actuation of nanomechanical optical fibers with integrated electrodes. A fiber structure that allows for control of the optical properties by mechanical reconfiguration through nanometer-range core movements has already been demonstrated before[13]. For electrostatic actuation of the fiber, charged electrodes are embedded in the fiber cladding. These generate a non-uniform electric field inside the fiber which polarizes the fiber cores and generates forces on them. At small separations between the cores, the dipole-dipole interaction between the two cores is found to be the dominant force, while at larger separations the interaction with the external field dominates. By using a simplified semi-analytical model we investigated the force dependence on the core dimensions and on the dielectric material properties. In particular we have shown that cores made of a glass with high dielectric permittivity (such as lead silicate glass) will experience higher electrostatic forces than silica glass cores. To increase the forces acting on the cores and hence their displacement, we suggested geometries with three and four electrodes around the central air hole. In particular, the quadrupole geometry was shown as the most promising design. Our results suggest that core displacements in the nanometer-range can be generated. As an example, we simulated the possibility of all-fiber optical switching in a 10cm long fiber with an operating voltage of 25 - 30V.

We also reported the fabrication process of dual core fibers with integrated electrodes. A multi-material fiber draw technique is employed for fabricating a fiber with a well-defined dual core structure in the middle and four continuous metal electrodes in the cladding. However, the central mechanical part of the first fiber appears to be too stiff to allow for electrostatically induced reconfiguration. Further improvement of the fabrication method will focus on controlling the dimensions of the fiber central structure. In particular a method of reducing the stiffness of the supporting membranes by making them thinner and longer will be developed.

REFERENCES

[1] Craighead, H.G., “Nanoelectromechanical systems,” Science 290, 1532-1535 (2000).

[2] Wu, M.C., Solgaard, O. and Ford, J.E., “Optical MEMS for lightwave communication,” J. Lightw. Technol. 24, 4433-4454 (2006).

[3] Ollier, E., “Optical MEMS devices based on moving waveguides” IEEE J. Sel. Top. Quant. Electron. 8, 155-162 (2002).

[4] Srikar, V.T. and Spearing, S.M., “Material selection for microfabricated electrostatic actuators,” Sens. Actuators A 102, 279-285 (2003).

[5] Moser, R., Wüthrich, R., Sache, L., Higuchi, T. and Bleuler, H., “Characterization of electrostatic glass actuators,” J. Appl. Phys. 93, 8945-8951 (2003).

[6] Lenssen, B. and Bellouard, Y., “Optically transparent glass micro-actuator fabricated by femtosecond laser exposure and chemical etching,” Appl. Phys. Lett. 101, 103503 (2012).

[7] Fokine, M., Nilsson, L.E., Claesson, Ã., Berlemont, D., Kjellberg, L., Krummenacher, L. and Margulis, W., “Integrated fiber Mach-Zehnder interferometer for electro-optic switching,” Optics Letters 27, 1643-1645 (2002).

[8] Yu, Z., Margulis, W., Tarasenko, O., Knape, H. and Fonjallaz, P.Y., “Nanosecond switching of fiber Bragg gratings,” Opt. Express 15, 14948-14953 (2007).

[9] Chesini, G., Cordeiro, C.M.B., de Matos, C.J.S., Fokine, M., Carvalho, I.C.S. and Knight, J.C., “All-fiber devices based on photonic crystal fibers with integrated electrodes,” Opt. Express 17, 1660-1665 (2009).

[10] Sazio, P.J.A., Amezcua-Correa, A., Finlayson, C.E., Hayes, J.R., Scheidemantel, T.J., Baril, N.F., Jackson, B.R., Won, D.-J., Zhang, F., Margine, E.R., Gopalan, V., Crespi, V.H. and Badding, J.V., “Microstructured optical fibers as high-pressure microfluidic reactors,” Science 311, 1583-1586 (2006).

[11] Bayindir, M., Sorin, F., Abouraddy, A.F., Viens, J., Hart, S.D., Joannopoulos, J.D. and Fink, Y., “Metal-insulator-semiconductor optoelectronic fibres,” Nature 431, 826-829 (2004).

[12] Lee, K., Henry, P., Simon, F. and Blows, J.L., “Drawing of optical fiber with internal co-drawn wire and conductive coating and electro-optic modulation demonstration,” Photonics Technology Letters, IEEE 18, 914-916 (2006).

[13] Lian, Z., Horak, P., Feng, X., Xiao, L., Frampton, K., White, N., Tucknott, J.A., Rutt, H., Payne, D.N., Stewart, W. and Loh, W.H., “Nanomechanical optical fiber,” Opt. Express 20, 29386-29394 (2012).

[14] Lian, Z., Horak, P., Feng, X., Xiao, L., Frampton, K., White, N., Tucknott, J.A., Rutt, H., Payne, D.N., Stewart, W. and Loh, W.H., "Nanomechanical functionality of dual core fibres," Optical Fiber Communication Conference (OFC) 2013, Anaheim, CA, USA.
[15] Akihama, Y. and Hane, K., "Single and multiple optical switches that use freestanding silicon nanowire waveguide couplers," Light Sci. Appl. 1, e16 (2012).
[16] Pruessner, M.W., Amarnath, K., Datta, M., Kelly, D.P., Kanakaraju, S., Ho, P.-T. and Ghodssi, R., "InP-based optical waveguide MEMS switches with evanescent coupling mechanism", J. Microelectromech. Syst. 14, 1070-1081 (2005).
[17] Kaajakari, V., [Practical MEMS], Small Gear Publishing (2009).
[18] Lee, M.M. and Wu, M.C., "Tunable coupling regimes of silicon microdisk resonators using MEMS actuators", Opt. Express 14, 4703-4712 (2006).
[19] Podoliak, N., Lian, Z., Loh, W.H. and Horak, P., "Design of dual-core optical fibers with NEMS functionality", Opt. Express 22, 1065-1076 (2014).
[20] Jones, T.B., "Basic theory of dielectrophoresis and electrorotation," IEEE Eng. Med. Biol. Mag. 22, 33-42 (2003).